

Supplementary Information

Cobalt Complexes Tuned by Anderson-type Polyoxometalates and Bis-amide Derivative Ligands Featured with 'V'-like Connector for Efficient Ampere Sensing and Visible-light Catalytic Reduction for Cr(VI)

Yue Zhang, Xiang Wang, Yue Wang, Na Xu and Xiu-Li Wang*

College of Chemistry and Materials Engineering, Professional Technology Innovation Center of Liaoning Province for Conversion Materials of Solar Cell, Bohai University, Jinzhou 121013, P. R. China

Preparation of organic ligands

Synthesis of L¹

Nicotinic acid (4.92 g, 0.04 mmol) and 4,4-diaminodiphenylmethane (3.96 g, 0.02 mmol) were placed a 250 mL three-necked flask containing pyridine (60 mL). After stirring for 30 min, triphenyl phosphate (12.3 g, 0.04 mol) was added slowly, and the mixture was refluxed for 10 hours. After cooling to room temperature, a white precipitate L¹ was obtained. The solid was filtered and washed with ethanol. The structure was determined by ¹H NMR and ¹³C NMR analysis (Fig. S2). ¹H NMR (400 MHz, DMSO-*d*₆) δ 10.80 (s, 2H), 9.14 (d, *J* = 1.3 Hz, 2H), 8.79 (d, *J* = 4.4 Hz, 2H), 8.33 (d, *J* = 8.0 Hz, 2H), 7.99 (d, *J* = 8.6 Hz, 4H), 7.81 (d, *J* = 8.5 Hz, 4H), 7.63–7.57 (m, 2H). ¹³C NMR (100 MHz, DMSO-*d*₆) δ 193.98, 165.02, 152.82, 149.24, 143.19, 136.10, 132.91, 131.28, 130.79, 124.00, 119.91.

Synthesis of L²

The synthesis process of L² was similar to that of L¹, except 4,4'-diaminodiphenylketone (4.24 g, 0.02 mmol) in place of 4,4-diaminodiphenylmethane as original material. White powder of L² were obtained. The structure was determined by ¹H NMR and ¹³C NMR analysis (Fig. S2). ¹H NMR (400 MHz, DMSO-*d*₆) δ 10.42 (s, 1H), 9.09 (d, *J* = 1.0 Hz, 2H), 8.75 (d, *J* = 4.5 Hz, 2H), 8.28 (d, *J* = 8.0 Hz, 2H), 7.69 (d, *J* = 8.3 Hz, 4H), 7.60–7.52 (m, 2H), 7.23 (d, *J* = 8.2 Hz, 4H), 3.91 (s, 2H). ¹³C NMR (100 MHz, DMSO-*d*₆) δ 164.31, 152.49, 149.08, 137.48, 137.28, 135.85,

131.04, 129.31, 123.92, 120.96.

Cr(VI) reduction calculation

The photocatalysis efficiency of complexes **1–4** for Cr(VI) reduction was calculated by using the standard equation:¹

$$\text{Cr(VI) reduction efficiency (\%)} = \left[\frac{A_0 - A_t}{A_0} \right] \times 100 \quad (1)$$

Here, A_0 is the initial solution absorbance, and A_t is the solution absorbance at reaction time t (min).

Table S1 Crystallographic data of complexes **1–4**.

Complex	1	2	3	4
Empirical formula	C ₅₀ H ₅₃ AlCo ₂ Mo ₆	C ₅₀ H ₅₈ Co ₂ Mo ₆ N ₈	C ₅₀ H ₆₈ Al ₂ Co ₂ Mo	C ₅₀ H ₅₄ Co ₂ Mo ₆ N ₈
Formula weight	1998.48	2168.14	3112.12	2196.11
Crystal system	Triclinic	Triclinic	Triclinic	Triclinic
Space group	<i>P</i> Error!	<i>P</i> Error!	<i>P</i> Error!	<i>P</i> Error!
a (Å)	6.8930(5)	8.9146(11)	12.4682(5)	8.7713(19)
b (Å)	11.8860(10)	10.3622(13)	12.4968(5)	10.978(3)
c (Å)	19.7450(16)	18.449(2)	14.3152(6)	18.101(4)
α (°)	106.693(2)	87.576(3)	81.7570(10)	81.880(4)
β (°)	90.862(2)	86.380(3)	80.9080(10)	83.858(4)
γ (°)	99.792(2)	78.615(3)	75.0090(10)	75.321(4)
V (Å ³)	1523.5(2)	1666.5(4)	2115.19(15)	1664.6(6)
Z	1	1	1	1
Dc (g cm ⁻³)	2.178	2.160	2.434	2.191
μ (mm ⁻¹)	1.841	2.107	2.236	2.113
F (000)	984	1060	1500	1072
Reflection collected	10071	12408	15697	9133
Unique reflections	6438	8272	10429	5876
parameters	466	476	633	479
R _{int}	0.0438	0.0671	0.0235	0.0476
GOF	1.019	0.920	1.008	0.936
R _I ^a [I ≥ α(I)]	0.0557	0.0617	0.0356	0.0452
wR ₂ ^b (all date)	0.1486	0.1738	0.0828	0.1066

$$^a R_I = \sum ||F_o| - |F_c|| / \sum |F_o|; \quad ^b wR_2 = \sqrt{\sum [w(F_o^2 - F_c^2)^2] / \sum [w(F_o^2)^2]}^{1/2}$$

Table S2. Selected bond distances (Å) and angles (°) of complexes **1–4**.

Complex 1

Co(1)-O(3)#2	2.152(6)	Co(1)-O(4)#2	2.159(5)
Co(1)-O(1)	2.129(5)	Co(1)-N(1)	2.083(7)
Co(1)-O(2)#1	2.208(6)	Co(1)-N(2)#3	2.124(7)
O(3)#2-Co(1)-O(2)#1	85.9(2)	N(1)-Co(1)-O(2)#1	179.7(3)
O(3)#2-Co(1)-O(4)#2	89.3(2)	N(1)-Co(1)-O(4)#2	90.0(2)
O(1)-Co(1)-O(3)#2	86.8(2)	N(1)-Co(1)-N(2)#3	95.2(3)
O(1)-Co(1)-O(2)#1	90.6(2)	N(2)#3-Co(1)-O(3)#2	168.0(3)
O(1)-Co(1)-O(4)#2	176.1(2)	N(2)#3-Co(1)-O(1)	85.4(3)
O(4)#2-Co(1)-O(2)#1	89.7(2)	N(2)#3-Co(1)-O(2)#1	85.1(3)
N(1)-Co(1)-O(3)#2	93.9(3)	N(2)#3-Co(1)-O(4)#2	98.5(2)
N(1)-Co(1)-O(1)	89.7(2)		

Symmetry codes for **1**: #1 -x, -y+1, -z #2 x+1, y, z #3 -x, -y, -z+1 #4 x-1, y, z

Complex 2

Co(1)-O(4)	2.062(7)	Co(1)-N(1)	2.135(11)
Co(1)-O(7)	2.100(7)	Co(1)-O(3W)	2.026(8)
Co(1)-O(2W)	2.084(7)	Co(1)-O(1W)	2.121(9)
O(4)-Co(1)-O(7)	90.2(3)	O(2W)-Co(1)-O(1W)	88.4(3)
O(4)-Co(1)-O(2W)	173.5(3)	O(3W)-Co(1)-O(4)	92.4(3)
O(4)-Co(1)-N(1)	91.5(3)	O(3W)-Co(1)-O(7)	177.1(3)
O(4)-Co(1)-O(1W)	89.9(3)	O(3W)-Co(1)-O(2W)	93.9(3)
O(7)-Co(1)-N(1)	91.5(3)	O(3W)-Co(1)-N(1)	89.8(4)
O(7)-Co(1)-O(1W)	87.5(3)	O(3W)-Co(1)-O(1W)	91.1(4)
O(2W)-Co(1)-O(7)	83.5(3)	O(1W)-Co(1)-N(1)	178.3(4)
O(2W)-Co(1)-N(1)	90.1(3)		

Symmetry codes for **2**: #1 -x+2, -y+2, -z

Complex 3

Co(1)-O(1W)	2.072(3)	Co(1)-O(2W)	2.050(3)
Co(1)-O(2)#1	2.107(3)	Co(1)-O(3)#2	2.113(3)
Co(1)-O(1)	2.053(3)	Co(1)-N(1)	2.088(4)
O(1W)-Co(1)-O(2)#1	89.99(11)	O(2W)-Co(1)-O(1W)	88.95(13)
O(1W)-Co(1)-O(3)#2	92.20(11)	O(2W)-Co(1)-O(2)#1	90.39(12)
O(1W)-Co(1)-N(1)	175.58 (13)	O(2W)-Co(1)-O(1)	175.29(13)
O(2)#1-Co(1)-O(3)#2	177.06(12)	O(2W)-Co(1)-O(3)#2	91.61(12)
O(1)-Co(1)-O(1W)	86.99(12)	O(2W)-Co(1)-N(1)	95.47(14)
O(1)-Co(1)-O(2)#1	92.00(11)	N(1)-Co(1)-O(2)#1	89.88(13)
O(1)-Co(1)-O(3)#2	86.16(11)	N(1)-Co(1)-O(3)#2	87.79(12)
O(1)-Co(1)-N(1)	88.60(13)		

Symmetry codes for **3**: #1 -x, -y, -z+1 #2 -x, -y+1, -z+1

Complex 4

Co(1)-O(1)	2.103(5)	Co(1)-O(1W)	2.122(6)
Co(1)-O(2)	2.088(6)	Co(1)-O(3W)	2.092(7)

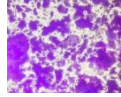
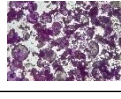

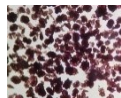
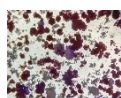
Co(1)-O(2W)	2.022(6)	Co(1)-N(1)	2.114(7)
O(1)-Co(1)-O(1W)	89.7(3)	O(2W)-Co(1)-O(1W)	90.5(3)
O(1)-Co(1)-N(1)	91.1(3)	O(2W)-Co(1)-O(3W)	98.8(3)
O(2)-Co(1)-O(1)	88.3(2)	O(2W)-Co(1)-N(1)	88.9(3)
O(2)-Co(1)-O(1W)	91.3(3)	O(3W)-Co(1)-O(1)	82.8(2)
O(2)-Co(1)-O(3W)	171.0(2)	O(3W)-Co(1)-O(1W)	90.4(3)
O(2)-Co(1)-N(1)	92.4(3)	O(3W)-Co(1)-N(1)	86.0(3)
O(2W)-Co(1)-O(1)	178.3(3)	N(1)-Co(1)-O(1W)	176.3(3)
O(2W)-Co(1)-O(2)	90.0(3)		

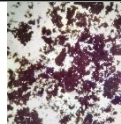
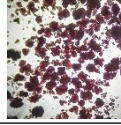
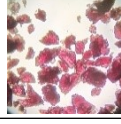
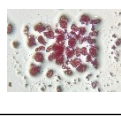
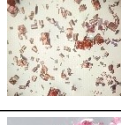
Symmetry codes for **4**: #1 -x+2, -y+2, -z

Table S3 Selected hydrogen bonding geometry (Å, °) for complexes **1–4**.

Complex	D–H···A	D–H / Å	H···A / Å	D···A / Å	D–H···A / °
1	N4–H4···O12	0.86	2.31	3.1241	158
	O2W–H2WB···O6	0.85	2.03	2.8272	155
2	N4–H4···O5	0.86	1.88	2.7398	176
	O2W–H2WB···O15	0.85	2.14	2.9003	149
3	O2W–H2WB···O15	0.85	2.14	2.9003	149
	O2W–H2WA···O3	0.85	1.81	2.5876	152
4	O2W–H2WA···O3	0.85	1.81	2.5876	152
	N4–H4···O15	0.86	2.19	3.0456	171

Table S4 Crystal states of complexes **1–4** in different solvents and composition.

Complex	Solvent type	Solvent composition	Magnification information	Crystalline state
1	H ₂ O: DMF	3:3	4.5*10	
	H ₂ O: DMA	3:3	4.5*10	
	H ₂ O: CH ₃ OH	3:3	4.5*10	
	H ₂ O: C ₂ H ₅ OH	3:3	4.5*10	
	H ₂ O: C ₂ H ₅ OH	3:5	4.0*10	

	H ₂ O: C ₂ H ₅ OH	2:6	4.0*10	
	H ₂ O: C ₂ H ₅ OH	5:3	4.0*10	
	H ₂ O: C ₂ H ₅ OH	6:2	4.5*10	
2	H ₂ O: C ₂ H ₅ OH	4:1	4.5*10	
3	H ₂ O: C ₂ H ₅ OH	4:6	4.5*10	
4	H ₂ O: C ₂ H ₅ OH	6:4	4.5*10	

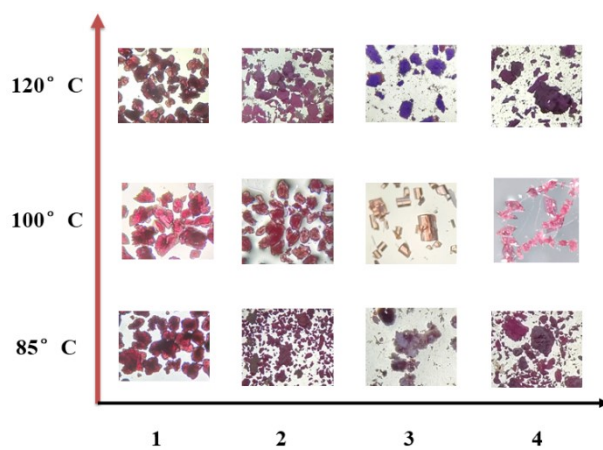


Fig. S1. Crystallization diagram of complexes 1–4 at different temperatures (Magnification information: 4.5*10).

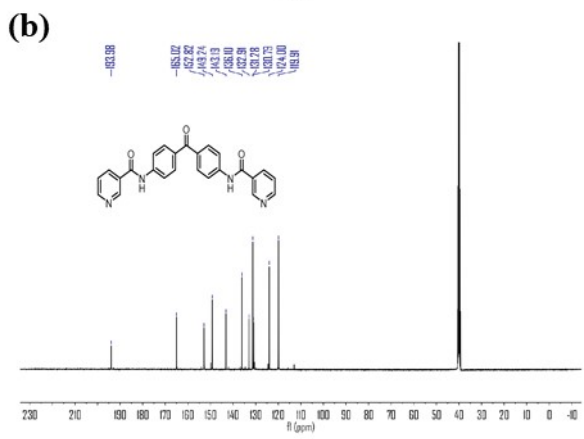
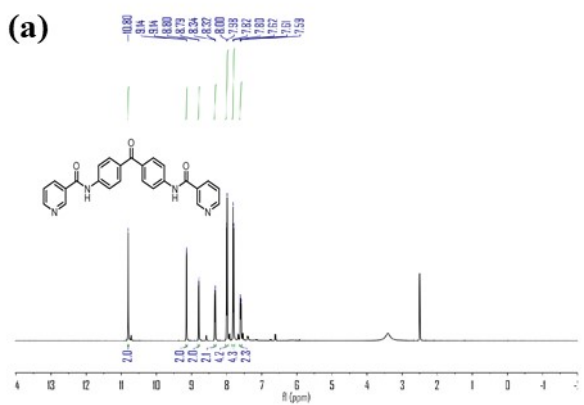
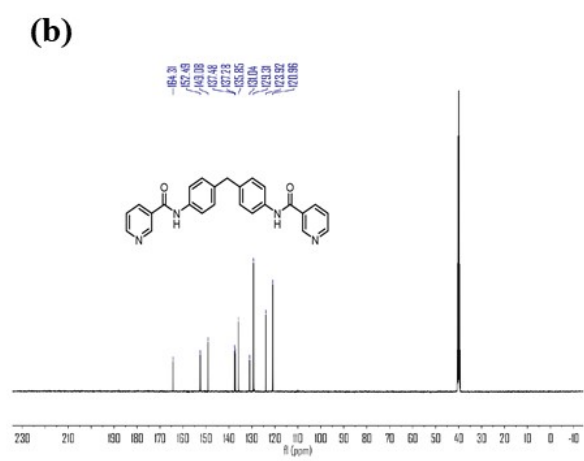
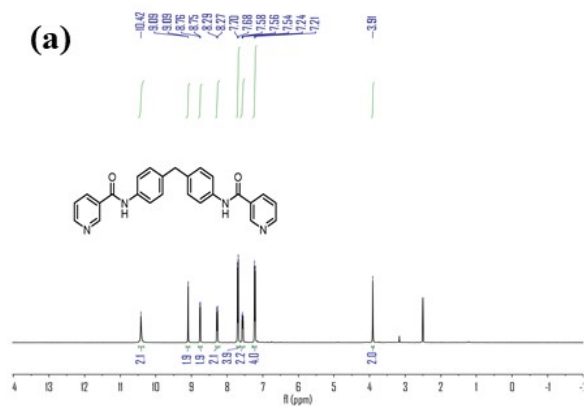


Fig. S2. ¹H and ¹³C NMR spectra of L¹ and L² in DMSO-*d*₆.

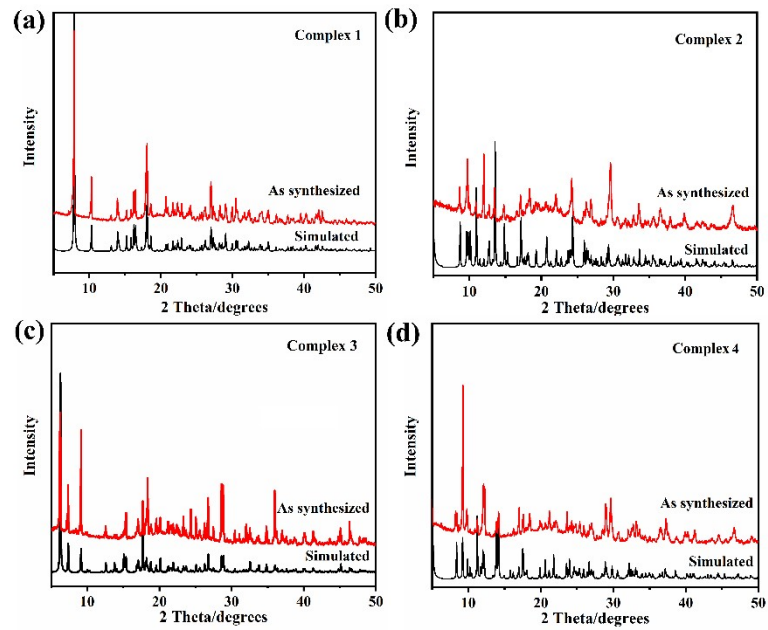


Fig. S3. The PXRD patterns of complexes 1-4.

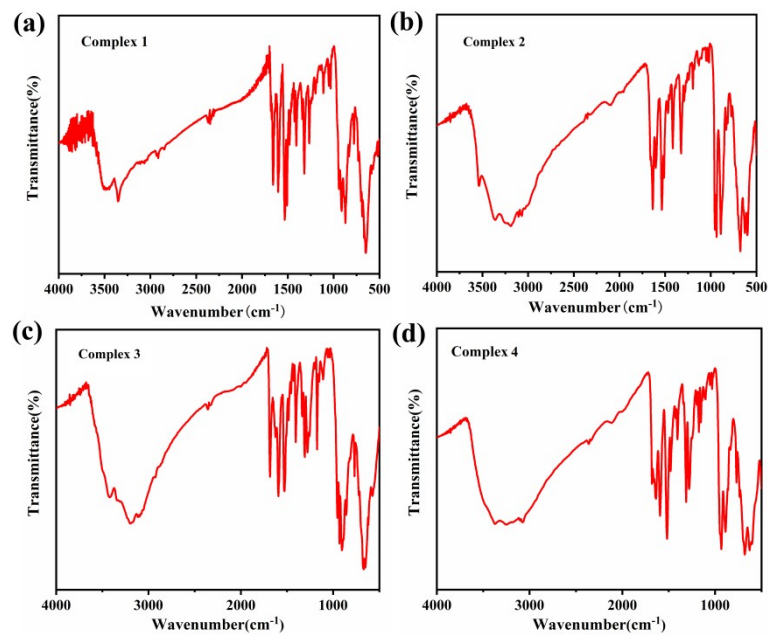


Fig. S4. The IR spectra of complexes 1-4.

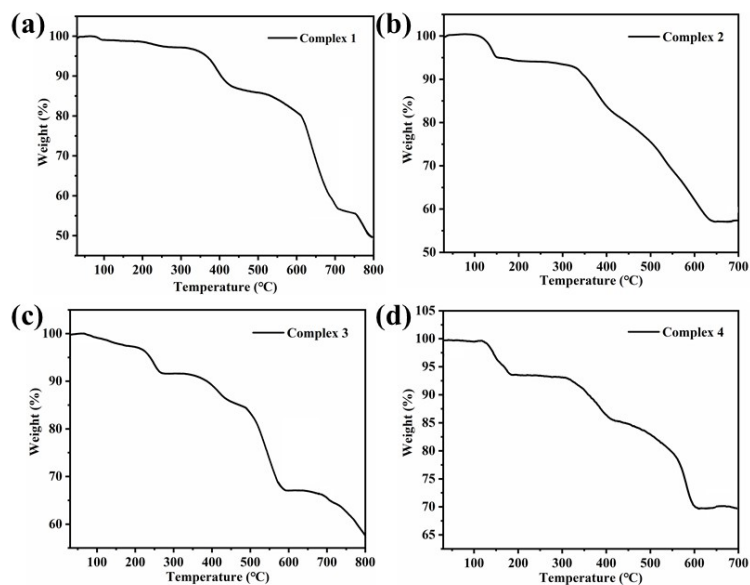


Fig. S5. The TG curves of complexes 1–4.

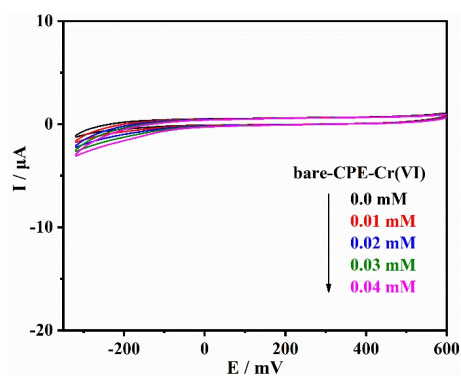


Fig. S6. The CV curves of bare-CPE in electrolyte solution containing Cr(VI) ions (scan rate: 60 mV s^{-1}).

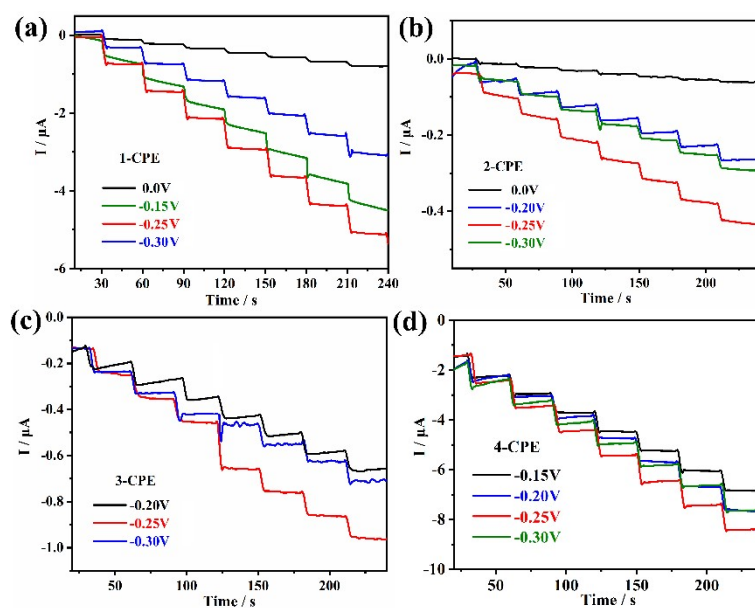


Fig. S7. The best potential of amperometric detection of Cr(VI) ions for 1–4-CPEs.

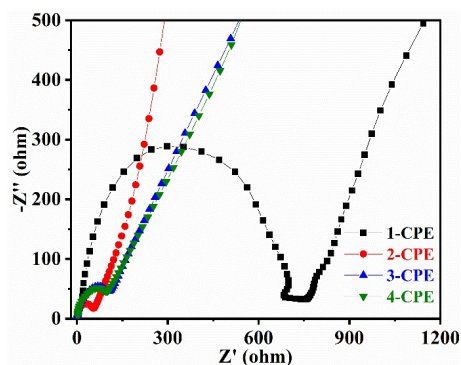


Fig. S8. Nyquist plots of 1–4–CPEs.

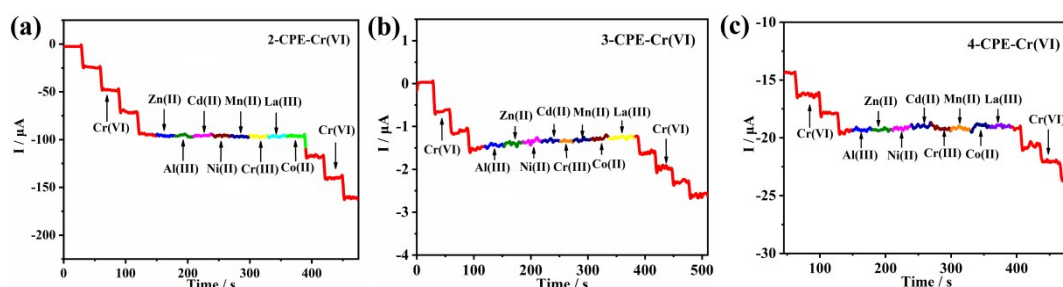


Fig. S9. Current response of 2–4–CPEs contains Cr (VI) ions with continuous addition of various metal ions (ions: 250 μM Cr^{3+} , Al^{3+} , Cd^{2+} , La^{3+} , Ba^{2+} , Co^{2+} , Ni^{2+} , Zn^{2+}).

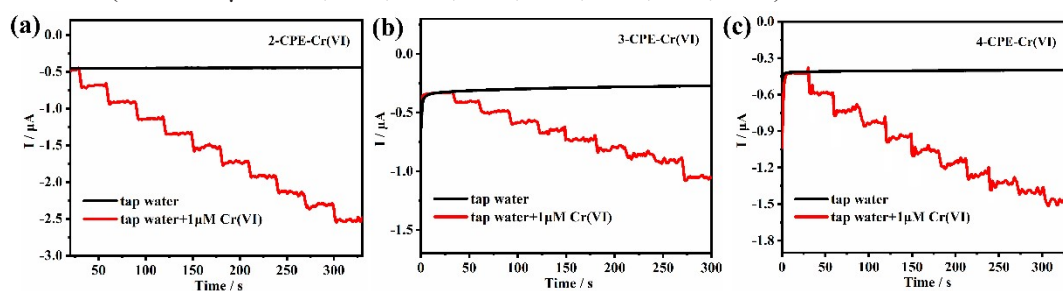


Fig. S10. Current response of 2–4–CPEs to detect trace Cr(VI) ions in tap water samples.

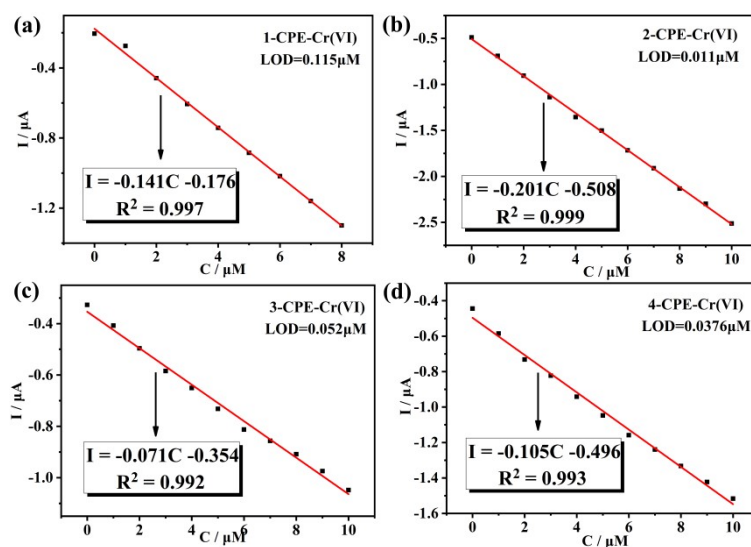


Fig. S11. Linear relationship between concentrations of Cr(VI) ions in real lake water sample and redox peak currents of 1–4–CPEs.

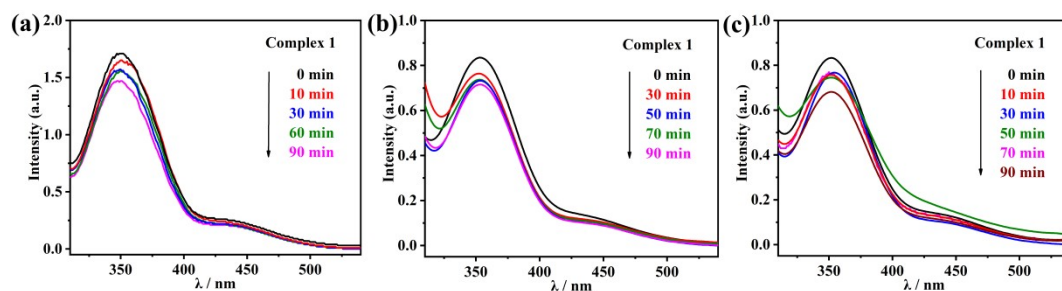


Fig. S12. Photocatalytic reduction of Cr(VI) ions: (a) without CH₃OH (b) without light (c) without catalyst.

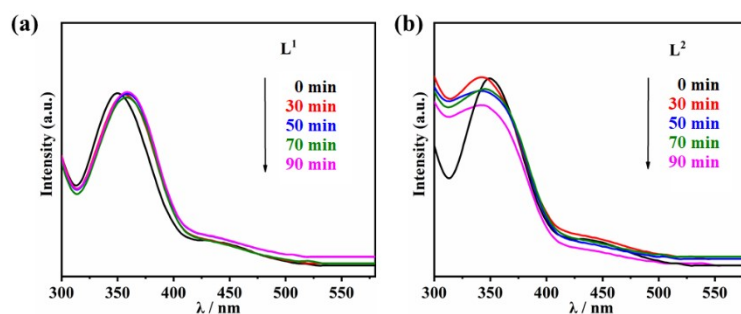


Fig. S13. Photocatalytic reduction of Cr(VI) with (a) L¹ and (b) L² as the catalysts under different irradiation times.

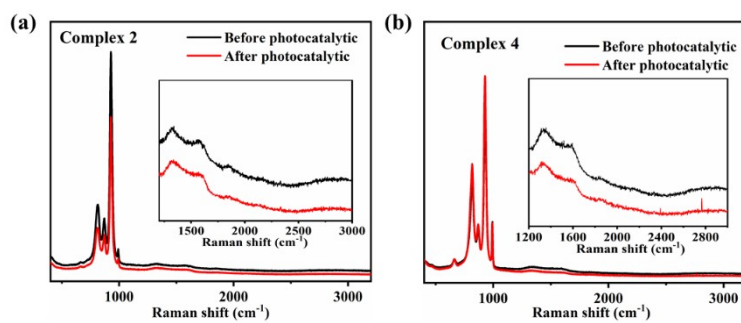


Fig. S14. Raman spectra of complexes 2 and 4.

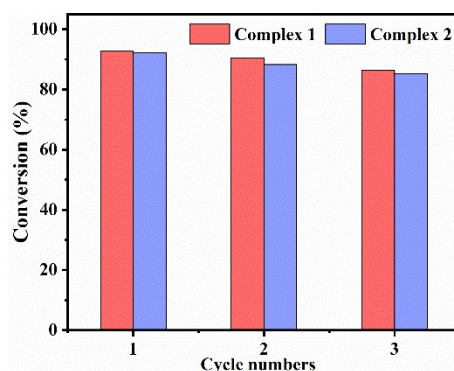


Fig. S15. Three cycle experiments of photocatalytic reduction of Cr(VI) ions solution with complexes 1–2 as catalyst.

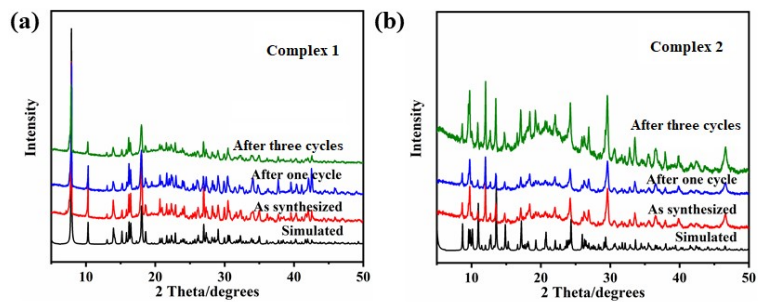


Fig. S16. The PXRD patterns of complexes 1–2 after photocatalysis.

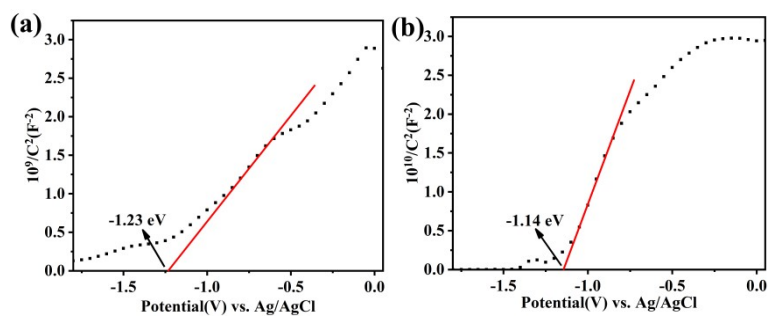


Fig. S17. Mott–Schottky plots in 0.1 M Na₂SO₄ aqueous solution at frequencies of 1000 Hz (a) Complex 1 (b) Complex 2.

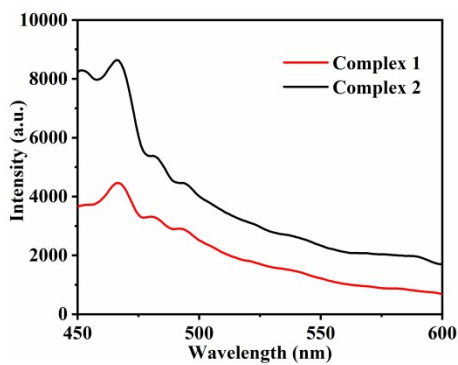


Fig. S18. Solid-state emission spectra of complexes 1–2 at room temperature.

1. X. R. Tian, Y. Q. Zhang, Y. Y. Ma, Q. Zhao, Z. G. Han, *Catal. Sci. Technol.*, 2020, **10**, 2593-2601.